Phase Ordering in Blend Films of Semi-crystalline and Amorphous Polymers

V. Ferreiro*, J. F. Douglas*, E.J. Amis, A. Karim

Polymers Division, National Institute of Standards and Technology, Gaithersburg, MD 20899, USA

SUMMARY: A combination of optical and atomic force microscopy (AFM) is used for probing changes in the morphology of polymer blend films that accompany phase ordering processes (phase separation and crystallization). The phase separation morphology of a "model" semi-crystalline (polyethyleneoxide or PEO) and amorphous (polymethylmethacrylate or PMMA) polymer blend film is compared to previous observations on binary amorphous polymer blend films of polystyrene (PS) and polyvinylmethylether (PVME). The phase separation patterns are found to be similar except that crystallization of the film at high PEO concentrations obscures the observation of phase separation. The influence of film defects (e.g., scratches) and clay filler particles on the structure of the semi-crystalline and amorphous polymer films is also investigated.

Introduction

The bulk properties of miscible fluid mixtures are characteristically *insensitive* to their microscopic fluid structure near the critical point for phase separation where the properties are governed by large scale fluctuations in the local fluid composition that occur similarly for most liquid mixtures at equilibrium. This situation changes, however, when the fluid mixture is brought into the two-phase region and the mixture begins to phase separate or when the fluid components crystallize. Under these unstable conditions, small-scale perturbations can grow to dominate the large scale structure of the mixture. Recent work has shown that the presence of micro-heterogeneities in phase separating blends can induce the development of compositional waves in the surrounding medium that tend to have the symmetry of the perturbing particles[1)]. The sensitivity of non-equilibrium crystallization to molecular structure (e.g., the shapes of snowflakes reflect the symmetry of the equilibrium crystallization morphology of water) is another well known phenomenon that can be expected to give rise to large scale structuring in semi-

 CCC 1022-1360/00/$ 17.50+.50/0

crystalline polymer films. Perturbations in unstable phase separating or crystallizing polymer blend films can be *amplified* rather than *washed out* at larger length scales. The beneficial aspect of this sensitivity of phase separation and other phase ordering processes to perturbations is that it offers substantial opportunities to *control* the morphology of blend films[1].

In previous work, we showed that the real space structure of polymer blend phase separation can be studied in considerable detail by forming nearly two-dimensional "symmetric" polymer films in which one of the polymer components segregates to *both* the solid substrate and the polymer-air boundaries[2-3]. The difference in the surface tension between the blend components causes the film surface to buckle in response to phase separation within the film[2]. This buckling provides a source of contrast in optical and AFM measurements, enabling high-resolution measurements of the dynamics of the ordering process in real space.

The present paper is a preliminary investigation of blend phase separation in the case where one of the components can crystallize. We cast films of crystallizable poly(ethylene oxide) (PEO) mixed in the casting solvent (chloroform) with an amorphous polymer poly(methyl methacrylate) (PMMA) and investigate these films combinatorially – vary film thickness, relative blend composition and the temperature of crystallization (T_c). We contruct a library of images for various conditions in this matrix of variables and show some representative morphologies revealed by this study. The influence of imperfections in the film and clay particles on the film structure is also considered. Clay particles were added to nucleate the crystallization and the relative polymer composition was adjusted to a range where symmetric polymer dendrites grow within the film. Separate papers focus on the dynamics of the dendritic growth and the morphologies that form at different polymer compositions[4]. The present paper is concerned with optical and atomic force microscopy (AFM) observations of film morphology changes arising from phase separation and crystallization.

Experimental

Sample Preparation. "Cloisite" (Montmorillonite; MON) clay particles were obtained from Southern Clay Products[5]. This clay mineral has exchangeable sodium

ions, and a cation exchange capacity of ca. 120 meq (milli-equivalent) per 100 g. PEO with average M_w = 200,000 g.mol^{-1} and PMMA of M_w = 120,000 g.mol^{-1} were purchased from Aldrich, USA. MON (1 g) and 50 ml of distilled water at 80°C were placed in 100-ml beaker, and 1 g of distearyldimethyl ammonium chloride was added to the solution. The mixture was stirred vigorously for 1h, and then filtered and rinsed three times with 100 ml of hot water to remove NaCl. After being washed with ethanol (50 ml) to remove any excess of ammonium salt, the product was freeze-dried, and kept in a vacuum oven at room temperature for 24h. The resulting organically modified montmorillonite (OMON) dispersed well in chloroform, although the unmodified montmorillonite (MON) did not disperse. The blend components (PEO/PMMA/OMON) were dissolved in chloroform at a total concentration of 1% by mass ratio, unless otherwise stated. Thin blend films were spin coated onto Si substrates (Semiconductor Processing Co., orientation (100), Type P) at a spin speed of 2000 rpm. This procedure results in films having a uniform thickness of ≈ 200 nm. Prior to spin coating, the Si wafers were "piranha-etched" to form a native SiO_2 surface layer. Reflective optical images were obtained with an optical microscope (OM) using a Nikon optical microscope with a digital Kodak MegaPlus CCD camera attachment.

Library preparation. Thickness gradients were prepared as follow. The cleaned wafer was placed on a robotic stage and secured, and a 3 cm wide knife-edge, angle at approximately 5°, subsequently placed 0.3 mm above the surface. A 50 μL of solution (mass fraction (2 to 5) % PEO/PMMA in chloroform) was placed under the knife-edge and the stage directed to move with constant acceleration to spread the solution. Solvent evaporation occurs in seconds after spreading and a thin film with thickness proportional to the velocity is produced. Control of initial thickness and slope is achieved by modifying the solution concentration and stage acceleration[6]. Resultant films are (20 to 35) mm in length and have nominal thickness variations of 80 nm range. The film thickness is characterized by 0.5 mm diameter spot-ellipsometry (with accuracy ± 1 nm at 500 nm film thickness) on a 2.5 mm grid across the gradient sample. A similar technique has been utilized to produce thickness gradients in a previous investigation of thin film dewetting[6]. The composition gradient film was prepared as describe by Meredith *et al.*[7].

High-throughput screening. The composition gradient sample or the thickness gradient sample were annealed on a linear T gradient heating stage, described elsewhere[7], over a large range of T, 25 °C < T < 250 °C. Optical microscope images and AFM images capture the evolution of the film morphologies as a function of T, film thickness and PMMA composition, ϕ_{PMMA}.

AFM experiments. All of the AFM measurements described below are carried out in air using a Dimension 3100 from Digital Instruments operating in a Tapping Mode™ [5]. Integrated silicon tips with a radius of curvature of about 10 nm and cantilevers (model TSEP) with a nominal spring constant 30 Nm^{-1} are used in our measurements. In the Tapping Mode™, the cantilever oscillates vertically at a drive frequency close to its resonance frequency and contacts the sample surface briefly in each cycle of oscillation. As the tip approaches the surface, the vibrational characteristics of the cantilever oscillation (e.g. amplitude, resonance frequency and phase angle) change due to the tip–sample interaction. "Height" images are obtained by using a feedback loop that keeps the amplitude at a constant value A_{sp} by vertically translating the sample with the piezoelectric scanner. The feedback loop is controlled by the set–point amplitude ratio $r_{sp} = A_{sp}/A_0$ where A_0 is the amplitude of free oscillation. The recorded "height" images are the vertical displacements of the piezoelectric scanner. Simultaneously, the phase of the cantilever oscillation relative to the signal exciting the piezoelectric driver can be measured. The corresponding recorded images represent the phase of the cantilever oscillation and are called "phase" images[8-10]. "Amplitude" images are obtained when the feedback loop is not connected. The amplitude can then vary and the resulting image reflects this variation. As mentioned by Aime et al.[11-13], it is essential to explore changes of the amplitude and phase as function of the tip–surface distance by making approach and retraction curves. These curves allow us to understand the origin of the contrast in both the "height" and "phase " images. Michel[10] has shown that the images of the surface of a triblock copolymer, PS–PI–PS, obtained in the repulsive interaction mode, exhibit a contrast that is due to change of the local mechanical properties. By varying the experimental parameters, the contrast of both "height" and "phase" images can be monitored and good contrast can be achieved. As an example, for a set–point amplitude ratio r_{sp} = 0.95 and a drive frequency (F) of 263.5 KHz, the contrast varies with the free

amplitude A_0. For example, both "height" and "phase" images show similar contrast for A_0 = 28.3 nm [same localization of the black (PI, elastomer) and white (PS, glassy) areas; lateral resolution is also the same]. For A_0 = 10.6 nm, the contrast of the "height" images is weak while the contrast of the "phase" images is enhanced and the lateral resolution is significantly increased. Thus, the local mechanical properties are imaged with the best contrast using the "phase" mode with a small free amplitude A_0 in the case of this triblock copolymer material. In the following work, different values of the free amplitude A_0 and set–point amplitude ratios r_{sp} have been used, depending on the material and the type of measurement, topographical or mechanical.

Results and Discussion

There have been several previous studies of blends of PEO and PMMA, encompassing mixtures of components of various molecular weights, and this blend is usually indicated to be miscible over a wide temperature range[14-16]. However, phase separation indicating a lower critical solution temperature (LCST) has been reported in PEO-PMMA films at the critical temperature of about 350 °C [17-18]. A phase separated morphology is observed in our cast films, that disappears above a temperature-composition locus that resembles an upper critical solution temperature (UCST) cloud point curve[19] (see Table 1 and Fig. 1 below).

Table 1. Polymer Crystallization Parameters

	T_c (°C)	T_m (°C)	T_g (°C)	χ
PEO	53	67	- 60	0.81
80/20	48	65	- 27	0.66
60/40	40	60	-11	0.42
50/50	36	58	5	0.31
40/60	-	59	25	0.11
20/80	-	-	65	-
PMMA	-	-	108	-

Table 1: Characteristics of the films, crystallization temperature (T_c), melting temperature (T_m), glass temperature (T_g) and blend crystallinity (χ).

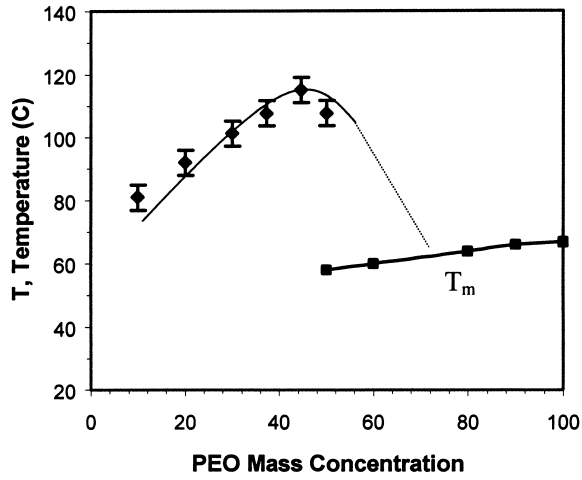

Figure 1: Phase diagram of PEO/PMMA blend thin film spun cast from chloroform. The phase boundary is associated with the temperature where the film become smooth (an AFM "cloud point curve")[3]. The phase separation process is obscured by crystallization at high PEO mass concentration and the dotted line shows the inaccessible extension of the phase boundary.

We estimate the UCST critical temperature (T_c) and the critical composition (ϕ_c) by this method to equal, $T_c \approx 105$ °C and $\phi_c \approx 0.55$. Previous determinations of cloud point curves of relatively thick PEO/PMMA polymer films cast from chloroform indicate T_c = 92 °C and $\phi_c = 0.53$ for a PEO-PMMA blend having molecular masses of $M_{w\,PEO} = 4.10^4$ g.mol^{-1} and $M_{w\,PMMA} = 10^5$ g.mol^{-1} and $T_c = 108$ °C and $\phi_c = 0.62$ for molecular masses of $M_{w\,PEO} = 10^6$ g.mol^{-1} and $M_{w\,PMMA} = 10^6$ g.mol^{-1} [20]. It should be appreciated that a small amount of residual solvent in the spun cast film could influence the phase separation behavior. However, this complicates the determination of temperature range where phase separation occurs, but does not change the qualitative nature of the phenomenon under investigation.

Phase Separation in Ultrathin Films

Polymer blends characteristically tend to phase separate due to the low entropy of mixing leading to a wide range of film morphologies. For thicker films (~500nm), it is usual for one of the components to segregate to the substrate and air surface, leading to the development of oscillatory "surface-directed" composition waves that become damped with increasing distance from the film surface. In films thinner than the wavelength of these surface induced compositional oscillations, it is possible for phase separation to occur laterally within the plane of the film. The interfacial tension variations that accompany phase separation lead to a buckling of the film surface[1-2]. AFM has been previously utilized to study the kinetics of phase separation in these "ultra-thin" films[1-2].

Phase Separation in Binary Amorphous Versus Semi-crystalline and Amorphous Polymer Blends

The morphology of polyethylene oxide (PEO) crystallization in a thin film geometry can be "tuned" through spherulitic, seaweed, dendritic and diffusion-limited aggregation (DLA) of crystallization forms through the adjustment of PEO composition and the degree of supercooling. These interesting crystallization morphologies are discussed in a separate paper[21], and here we focus specifically on dendritic crystallization in polymer blend films. We note that while the observation of polymer dendritic crystallization is rather unusual, dendrites grown from solvents have been observed previously[22-25]. There has also been a recent report of directional PEO crystallization within the holes of a dewetting PEO film[25].

Figures 2a-b correspond to AFM images showing changes in morphology that accompany composition changes in two model blends; one semi-crystalline/amorphous (PEO/PMMA) and the other amorphous/amorphous (PS/PVME)[3,26]. In the amorphous/amorphous blend, we go from a hole morphology through a labryinthine spinodal decomposition phase separation pattern ("spinodal pattern") to a film covered by "bumps". The presence of hole in the blend morphology is due to the component having the smaller surface tension and the bumps correspond to a minority component with a higher surface tension within the film. The bumps regime is not observable in the case of the PEO/PMMA blend because the crystallization of PEO overwhelms the phase

separation process (See Fig. 1). Instead, the lamellae structure of the PEO-rich crystallites are apparent in films having a high PEO concentration.

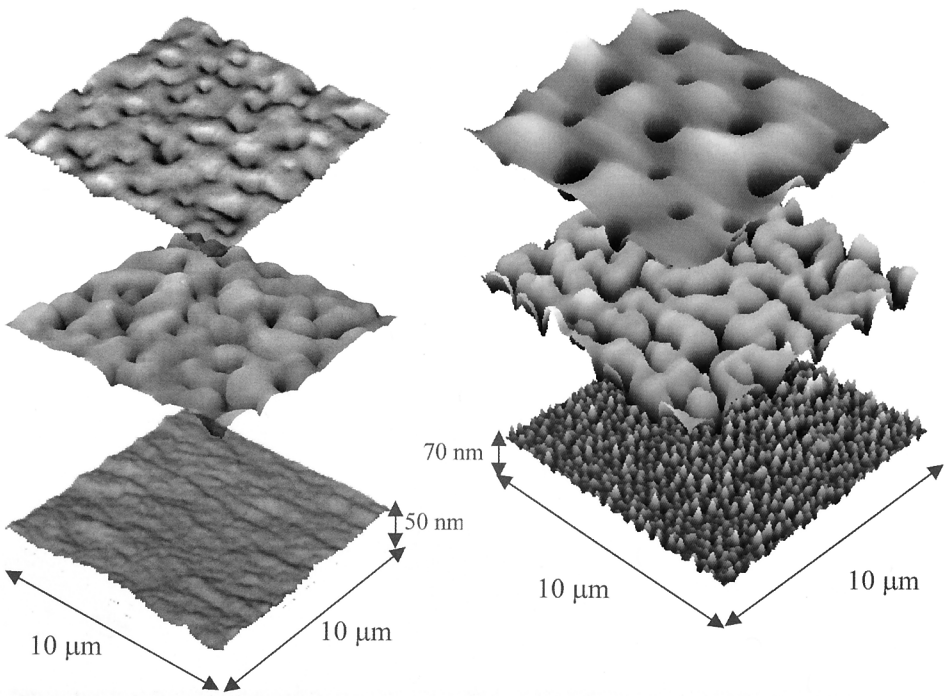

a. **b.**

Figure 2: Effect of blend composition on the morphology of two model systems; semi-crystalline/amorphous blend (PEO/PMMA) and amorphous/amorphous blend (PS/PVME). a) 3-Dimensional (Relief) AFM images of the evolution of the phase separated morphology of PEO/PMMA from 10/90 relative mass fraction of PEO at the top, in the middle 35/65 (near critical composition) and to 80/20 at the bottom. b) 3-Dimensional (Relief) AFM images of the evolution of the phase separated morphology of PS/PVME blend from 55/45 relative mass of PS at the top, 35/65 in the middle (near critical composition) to 10/90 at the bottom.

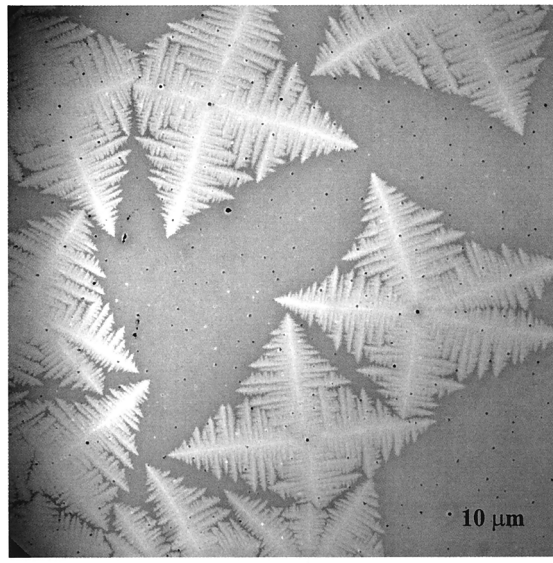

a.

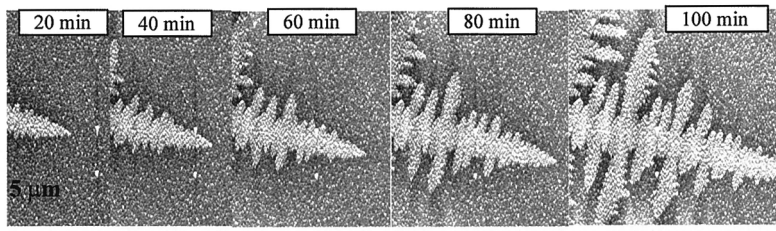

b.

Figure 3: Symmetric dendritic morphology of a (30/70) PEO/PMMA blend film crystallized at 32 °C during 2 hours. a) Optical image shows the regular "star-like" morphology of the dendrites. b) In-situ crystallization under AFM showing the progressive growth of the dendrite tip.

Figure 3a shows the growth of polymer dendrites in a (30/70) relative mass composition (PEO/PMMA) blend. The dark features (≈ 1 μm in size) in the optical micrograph correspond to agglomerates of clay particles that "seed" the crystallization.

The dendrites grow in a regular "star-like" morphology. Fig. 3b shows AFM images of the progressive growth of the dendrite tip during an in-situ crystallization. The crystallization rate (0.17 μm/min) is relatively slow in comparison to typical values for metals and small molecule liquids and it is possible to track the fine detail of the crystallization morphology with high resolution using AFM.

Effect of Temperature on Crystallization Morphology.

After spin-casting the films, we heat them to 100 °C over 5 minutes in order to melt the PEO. The films are then cooled down to the desired crystallization temperature.

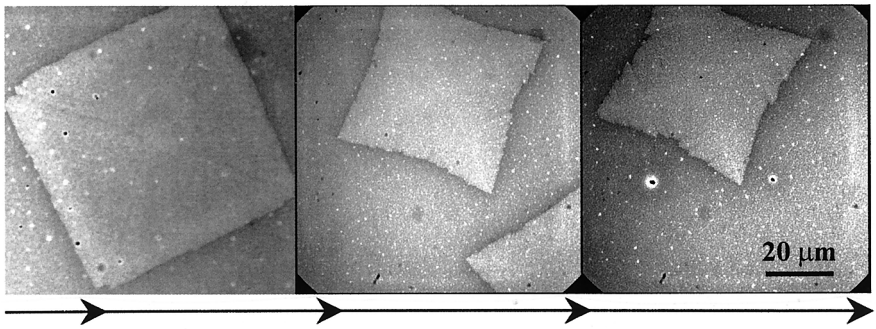

Figure 4: Parameters influencing the morphology of PEO/PMMA blend. Optical images show the evolution of the dendrite morphology with the degree of undercooling, ΔT.

Figure 4 shows topographic images of a PEO/PMMA film crystallizing at different temperatures. The film thickness h is approximately constant (h = 150 nm) and the clay concentration was 5 % of the polymer blend mass. A nearly square (equilibrium morphology) crystal forms for low undercooling (10 °C) and we observe a change to a dendritic morphology at high undercooling (35 °C). Under identical crystallization conditions (polymer composition, temperature, film thickness) there are no crystallization patterns in the absence of clay particles to nucleate the crystallization. The films are "excitable", however, and scratching a (30/70) PEO/PMMA blend film induces the formation of a dendritic wavefront that propagates to cover the film (Fig. 5).

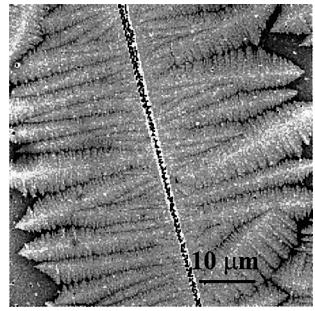

Figure 5: Optical image showing a dendritic wavefront propagating perpendicularly to a scratch. Crystallization conditions are the same as in Fig. 3, except there is no clay added to the polymer.

Dust particles were also observed to initiate dendrite growth in PEO/PMMA blend films without the clay filler. We then see that film imperfections can have a large influence on the properties of semi-crystalline blend films.

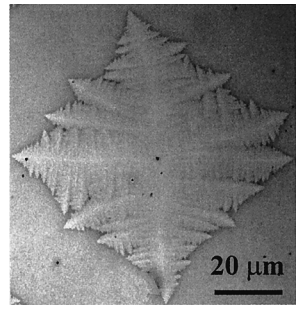

Figure 6: Optical image showing increase in the number of dendrite branches at a higher concentration of clay (10% by mass).

Clay particles can have other effects than simply nucleating the polymer crystallization. At higher clay concentrations (> 5 %), the interference between competiting growth centers (nucleating clay sites) can cause the dendrite arms to further

branch, leading to dendrites with an increased numbers of arms. We illustrate this effect in Fig. 6 for a 10 % mass fraction of clay where the relative PEO/PMMA blend composition is again fixed at (30/70). At clay concentrations below 5 %, we only observe dendrites having four arms (See Fig. 3) [21].

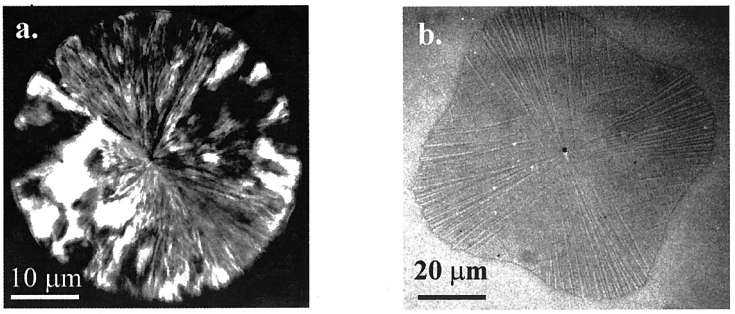

Figure 7: a) Optical image of a PEO spherulite crystallized at 58 °C during 2 hours. b) Optical image of a 45/55 relative mass ratio PEO/PMMA film crystallized at 32 °C for 2 hours.

At high PEO concentrations we obtain normal spherulitic growth (Fig. 7a), but we observe *distorted* spherulitic structures at a composition near where the crystal growth makes a transition from spherulitic to seaweed dendrite growth[4]. Fig. 7b shows this curious transition morphology which occurs for a 45/55 relative PEO/PMMA mass concentration. The growth pattern has the needle-like structure of a spherulite, but the front of the crystallization pattern is not circular.

Relation of Phase Separation Pattern to Dendritic Growth Pattern.

We next focus on the interplay between phase separation and crystallization, as revealed by an examination of the fine structure of the growing dendrite shown in Fig. 8a. The square region in the optical image of the dendrite shown in Fig. 8a is shown at higher resolution using AFM. This enlargement reveals a "granular" structure within the dendrite region. We enlarge the region shown by the square in the (coarse scale) AFM image and observe the local film structure in the vicinity of the dendrite. At this fine scale

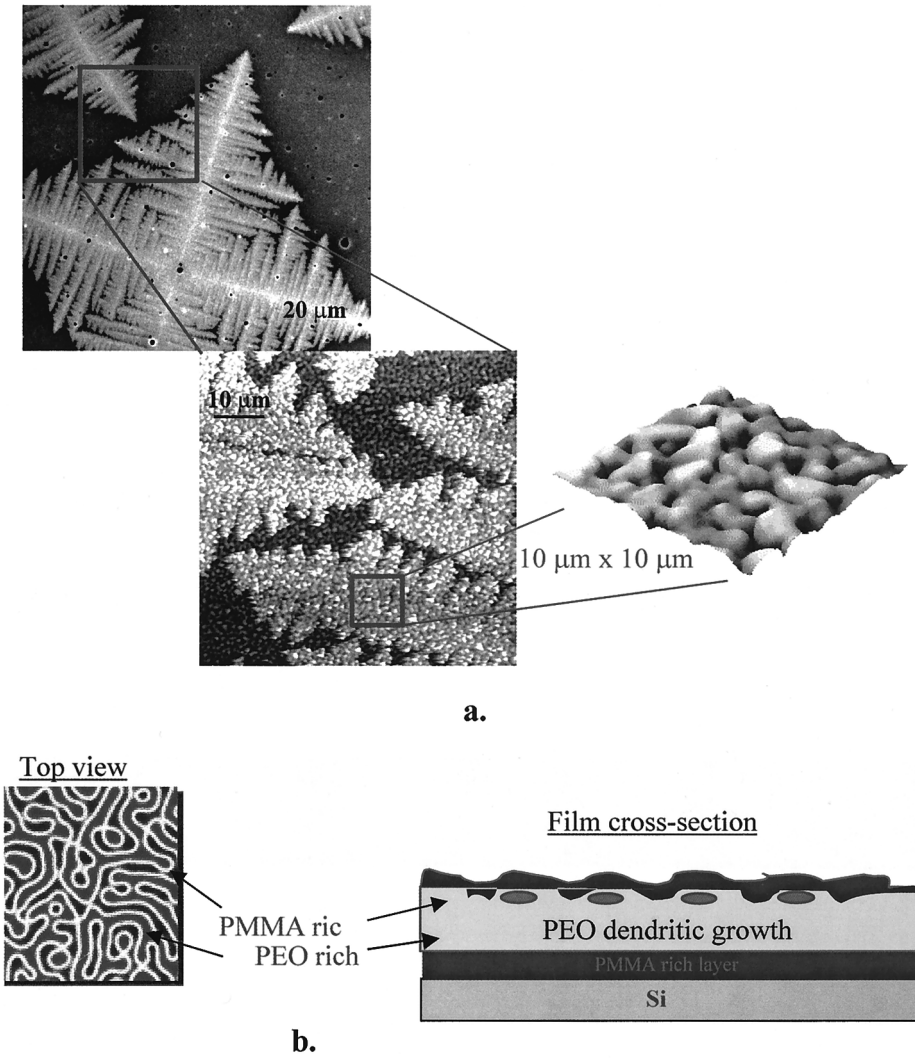

Figure 8: Interplay between phase separation and crystallization within the polymer dendrite a) Optical image of a dendrite crystallized at 32 °C for 2 hours. The AFM images reveal the "granular" structure within and outside the dendrite. b) Schematic view of the polymer crystallization in "sandwich" between surface layers enriched in PMMA.

[entire image dimension (10 μm x 10 μm)], we observe the undulatory structure of blend phase separation in an ultra-thin symmetric blend film[2-3]. This morphology is representative of previous studies of phase separation in blend films using AFM[3,27-29]. It is important to note that the film exhibits the same phase separation structure away from the dendrite, so that the phase separation pattern *does not* reflect a structure within the polymer dendrite. The whole surface of the film exhibits a pattern of microphase separation near the surface of the film. The crystallization apparently occurs well within the film and the phase separation pattern is limited to a thin skin near the polymer air-boundary. The PMMA segregates to both the solid substrate and the polymer-air substrates and the polymer crystallization and phase separation occur in the intervening blend sandwich between these layers (see Fig. 8b). The surface and interfacial tension differences between the PMMA and PEO rich phases cause the film thickness to undulate and thus provides a source of contrast in both optical and AFM measurements. These surface modulations are expected to be modified by crystallinity effects in semi-crystalline and amorphous polymer blends. Notably, we also observe the same undulatory phase separation morphology by simply eliminating the clay which nucleate the PEO dendrites. No dendrites form in the blend films without clay or film imperfections such as scratches. The local compositional enrichment caused by the clay or defects then appears to be important for nucleating polymer dendrites.

There is a subtlety to this heterogeneous nucleation process that was not originally anticipated in planning our measurements. The clay particles are nearly spherical in shape [average radius, R ~ 200 nm)] and have been treated ("modified") with surfactant to facilitate their dispersal in the polymer blend. We find that the clay particles do not disperse in the pure PEO, but rather segregate to the polymer-air boundary. The PEO films recrystallize into spherulites and appear similar to films without clay. This leads us to the question of how the clay particles could serve to nucleate crystallization in the PEO/PMMA blend. Previous work[1] has shown that the surface enrichment of one blend component about the particles leads to a *counter enrichment* of the other phase about the first layer. This wave-like pattern of composition about the filler particles is probably important for stimulating crystallization about the clay particles. Thus, it is not necessary

for an effective nucleating agent to have a favorable interaction with the crystallizing species in a polymer blend.

Conclusion

AFM is an important tool for probing the fine structure of multiphase materials. This method should help us to obtain an improved understanding of phase ordering in polymer materials – both equilibrium and dynamical properties. Such studies are important for developing a greater understanding of phase separation and crystallization in polymeric materials. Polymer systems are interesting for fundamental studies of phase ordering by AFM because of their large viscosity and because of the large time-scales normally found for phase ordering processes in these materials. We envision that AFM and related probe microscopes will become powerful tools for studying local property changes that occur in thin polymer materials.

References

1. B.P. Lee, J.F. Douglas, S.C. Glotzer, *Phys. Rev. E* **60**, 5812 (1999)
2. L. Sung, A. Karim, J. F. Douglas, and C.C. Han, *Phys. Rev. Lett.* **76**, 4368 (1996);
3. B. D. Ermi, A. Karim and J. F. Douglas, *J. Polym. Sci.* **36**, 191 (1998);
4. V. Ferreiro, J. Douglas, J. Warren, A. Karim, *Growth pulsations in dendritic crystallization*, submitted.
5. Certain commercial materials and equipment are identified in this article in order to specify adequately the experimental procedure. In no case does such identification imply recommendation by the National Institute of Standards and Technology, nor does it imply that the material or equipment identified is necessary the best available for this purpose
6. J.C. Meredith, A.P. Smith, A. Karim, E.J. Amis, *Macromolecules*, **33**, 9747 (2000)
7. J.C. Meredith, A. Karim, E.J. Amis, *Macromolecules*, **33**, 5760 (2000)
8. Magonov, S.N; Elings, V.; Wangbo, M.H. *Surf. Sci.* **389**, 201 (1997)
9. Magonov, S.N.; Cleveland, J.; Elings, V. *Surf. Sci.* **375**, 385 (1997)
10. Michel, D.; *PhD thesis*, Université de Bordeaux 1, France (1997)

11. Boisgard, R.; Michel, D.; Aimé, J.P.; *Surf Sci.* **401**, 199 (1998)
12. Aimé, J.P.; Michel, D.; Boisgard, R.; Nony, *L.; Phys Rev B* **59**,1829 (1999)
13. Nony, L.; Boisgard, R.; Aimé, J.P.; *J of Chemical Physics* **111**, 1 (1999)
14. M. Cortazar, M. E. Calahorra, G.M. Guzman, *Eur. Polym. J.* **18**, 165 (1982).
15. S.A. Liberman, A.D.S. Gomes, E.M. Macchi, *J. Polym. Sci., Polym. Chem. Ed.* **22**, 2809 (1984).
16. E. Martuscelli, M. Pracella, W.P. Yue, *Polymer* **25**, 1097 (1984).
17. S. Cimmino, E. Martuscelli, C. Silvester, *Polymer* **30**, 393 (1989).
18. A.C. Fernandes, J.W. Barlow and D.R. Paul, *J. Appl. Polym. Sci.* **32**, 5481 (1986);
19. K.E. Min, J.S Chiou, J.W. Barlow and D.R. Paul, *Polymer* **28**, 1721 (1987).
20. A.B. Burdin, A.A. Tager, *Vysol. Soed. Ser.* **B 37**, 850 (1995).
21. V. Ferreiro, J.F. Douglas, J. Warren, A. Karim, *Non-equilibrium pattern formation in the crystallization of polymer blend films*, submitted.
22. P.H. Till, *J. Polym. Sci.* **24**, 301 (1957);
23. P.H. Geil and D. H. Reneker, *J. Polym. Sci.* **51**, 569 (1961);
24. F. Khoury and J. D. Barnes, *J. Res. NBS* **78B**, 95 (1974);
25. G. Reiter and J. Sommer, *J. Chem. Phys.* **112**, 4378 (2000).
26. B.D. Ermi, A. Karim, J.F. Douglas and L. Sung, Polymer Preprint, PMSE, **11**, 606 (1997)
27. S. Affrosman, T. Kiff, S. O'Neill, R. Petrick, R. Richards, *Macromolecules*, **32**, 2721 (1999)
28. Bruder, F.; Brenn, R.; *Phys. Rev. Lett.* **69**, 624 (1992)
29. Slawecki, T.M.; *Ph.D. Thesis*, Pennsylvania State University, (1995)